arXiv:1402.4451v3 [quant-ph] 21 Feb 2014

Dynamical Casimir effect entangles artificial atoms

S. Felicetti,[1] M. Sanz,[1] L. Lamata,[1] G. Romero,[1] G. Johansson,[2] P. Delsing,[2] and E. Solano[1,3]

[1]*Department of Physical Chemistry, University of the Basque Country UPV/EHU, Apartado 644, E-48080 Bilbao, Spain*
[2]*Department of Microtechnology and Nanoscience (MC2), Chalmers University of Technology, SE-412 96 Göteborg, Sweden*
[3]*IKERBASQUE, Basque Foundation for Science, Alameda Urquijo 36, 48011 Bilbao, Spain*

(Dated: February 24, 2014)

The phenomenon of quantum fluctuations, consisting in virtual particles emerging from vacuum, is central to understanding important effects in nature—for instance, the Lamb shift of atomic spectra[1] and the anomalous magnetic moment of the electron[2]. It was also suggested[3] that a mirror undergoing relativistic motion could convert virtual into real photons. This phenomenon, denominated dynamical Casimir effect (DCE), has been observed in recent experiments with superconducting circuits[4,5]. Here, we show that the physics underlying the DCE may generate multipartite quantum correlations. To achieve it, we propose a circuit quantum electrodynamics (cQED) scenario involving superconducting quantum interference devices (SQUIDs), cavities, and superconducting qubits, also called artificial atoms. Our results predict the generation of highly entangled states for two and three superconducting qubits in different geometric configurations with realistic parameters. This proposal paves the way for a scalable method of multipartite entanglement generation in cavity networks through dynamical Casimir physics.

The appearance of a vacuum-mediated force between two perfectly conducting plates, known as the Casimir effect, is caused by a reduction of the density of electromagnetic modes imposed by the boundary conditions[6–8]. This leads to a vacuum radiation pressure between the mirrors that is lower than the pressure outside. The kinetic counterpart, namely, the dynamical Casimir effect, can be understood as a mismatch of vacuum modes in time. A moving mirror modifies the mode structure of the electromagnetic vacuum. If the mirror velocity, v, is much smaller than the speed of light, c, then the electromagnetic modes adiabatically adapt to the changes and no excitations occur. Otherwise, if the mirror experiences relativistic motion, changes occur nonadiabatically and the field can be excited out of the vacuum, generating real photons.

Beyond its fundamental interest, we may consider the study of the DCE as a resource for quantum networks and quantum simulations in the frame of quantum technologies. In circuit quantum electrodynamics, DCE photons have been created by modifying the boundary condition for the electromagnetic field[4]. In a similar experiment photons have also been created by modulating the effective speed of light[5]. Here, we investigate how to generate multipartite entangled states of two-level systems, also referred to as quantum bits (qubits), by means of varying boundary conditions. The scheme in Fig. 1a shows two cavities sharing a partially reflecting mirror and separately coupled to two single qubits. We assume that the cavity-qubit coupling strength is much larger than any decoherence rate in the system. In this context, we introduce the key concepts allowing the generation of highly-entangled two-qubit states, also known as Bell states[9], in circuit QED[10–12] (see Fig. 1b). Later on, we will also consider the generation of tripartite entanglement[13] and the scalability aspects of our proposal to multipartite systems (see Supplementary Information).

The Hamiltonian describing the system of Fig. 1a is composed of the sum of two Jaynes-Cummings (JC) interactions, and a time-dependent coupling between the field quadratures,

$$\mathcal{H} = \sum_{\ell=1}^{2}\left[\omega_\ell a_\ell^\dagger a_\ell + \frac{\omega_\ell^q}{2}\sigma_\ell^z + g_\ell\left(\sigma_\ell^+ a_\ell + \sigma_\ell^- a_\ell^\dagger\right)\right] + \alpha(t)\left(a_1^\dagger + a_1\right)\left(a_2^\dagger + a_2\right). \quad (1)$$

Here, $a_\ell^\dagger$, a_ℓ are the creation and annihilation operators of the bosonic modes representing the cavity fields, while σ_ℓ^z, $\sigma_\ell^\pm$ are the Pauli operators of qubits. The characteristic frequencies of the two cavities are denoted by ω_ℓ, while the qubit energies are ω_ℓ^q. The parameters g_ℓ and $\alpha(t)$ denote the cavity-qubit and cavity-cavity interaction strength, respectively.

The boundary condition at the border shared by the cavities is ruled by the central mirror position and by its reflection coefficient. Modulating these physical quantities results in a time dependence of the cavity frequencies ω_i and of the coupling parameter α. When the effective cavity length is oscillating with small deviations from its average value, we can still consider the system as a single-mode resonator (see Methods). In particular, if the cavity-cavity coupling parameter is a time-dependent function, $\alpha(t) = \alpha_0 \cos(\omega_d t)$ with $\omega_d = \omega_1 + \omega_2$ and $\alpha_0/\omega_i \ll 1$, the interaction effectively turns into a two-mode squeezing term (see Methods),

$$\alpha(t) X_1 X_2 \rightarrow \frac{\alpha_0}{2}\left(a_1^\dagger a_2^\dagger + a_1 a_2\right), \quad (2)$$

which generates pairs of entangled photons shared by the cavities. By means of the Jaynes-Cummings interaction, entanglement generated between both cavities may be transferred to both superconducting qubits. In fact, we will prove below that, under suitably designed conditions, maximal entanglement (Bell state) between the two qubits may be attained.

Nowadays, quantum technologies[14] offer several platforms to study fundamentals and applications of quantum theory. In particular, circuit QED[15–17] emerges as the strongest candidate to implement the proposed model in equation (1) satisfying the required parameter regime. In this framework, the cavities are constituted by coplanar waveguides that can be described by an equivalent LC circuit, as shown in Fig. 1b,c. The characteristic frequency of such devices is in the $2-10$ GHz

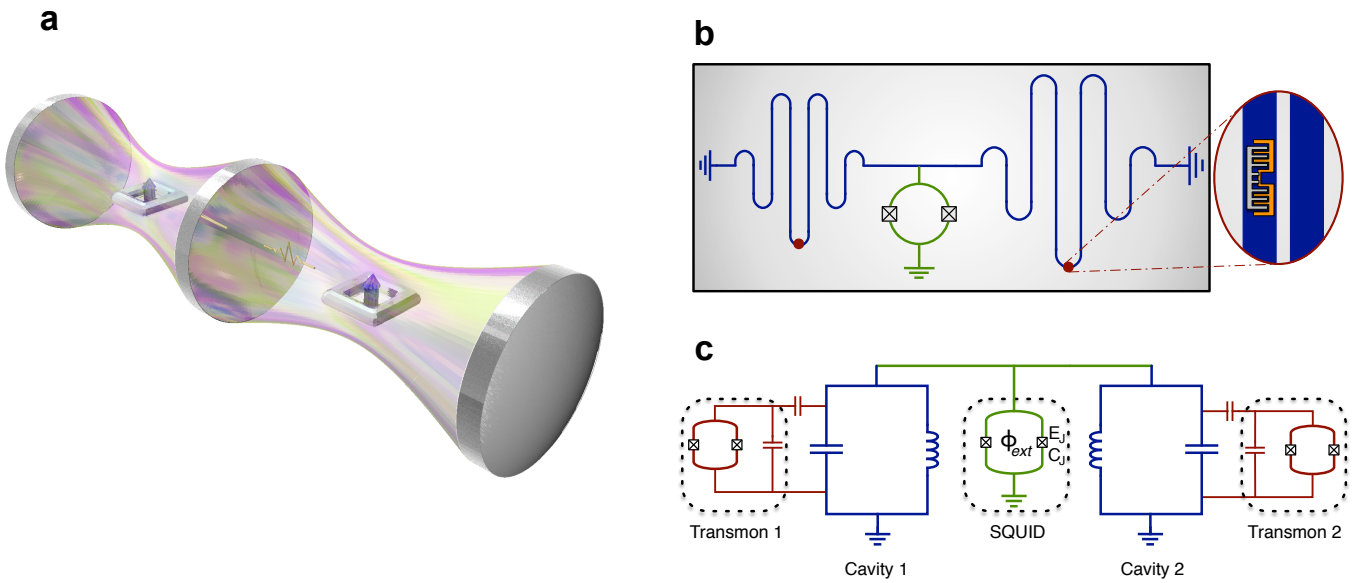

FIG. 1. **DCE and bipartite entanglement. a**, Quantum optical implementation of the model of equation (1): two cavities with a common partially-reflecting mirror, each one containing a two-level artificial atom in the strong-coupling regime. If the position and/or transmission coefficient of the central mirror is time-modulated, correlated photon pairs are generated and entanglement is transferred to qubits via the Jaynes-Cummings interaction. **b**, Such model can be implemented using two coplanar waveguides, grounded through a SQUID, containing two superconducting qubits. The blue lines represent two parallel strip lines of isolating material, where the superconducting region between them constitutes the coplanar waveguide. Each cavity interacts with a transmon qubit that is denoted by a red dot. Different resonator lengths result in distinct resonator frequencies. **c**, Circuit diagram for the previous scheme, where the cavities are effectively represented by LC resonators. We assume two identical Josephson junctions of the SQUID, while transmon qubits are constituted by two Josephson junctions shunted by a large capacitance. Notice that a modulation of the magnetic flux threading the SQUID induces a proportional variation of the effective resonator lengths, while in the system shown in box (a), moving the central mirror results in an opposite change of cavity lengths.

microwave regime. Each cavity can be coupled to a superconducting qubit built from Josephson junctions (JJs) to access charge[19], flux[20], or phase[21] degrees of freedom. Specifically, we propose the use of transmon qubits which have low sensitivity to charge noise and coherence times well above ten μs[22,30,31]. The moving mirror that couples both cavities (see Fig. 1a) can be implemented by means of a SQUID[23] device, namely, a superconducting loop interrupted by two JJs (see Fig. 1b), and threaded by an external flux $\phi_{\rm ext}$. The latter allows a fast modulation of the electrical boundary condition of cavities and their interaction.

Using off-the-shelf electronics, it is possible to produce magnetic fluxes that oscillate at the cavity characteristic frequencies. The upper limit to the speed of modulation is imposed by the SQUID plasma frequency defined as $\omega_p = \frac{1}{\hbar}\sqrt{8E_C E_J}$, where E_C is the charging energy, E_J the Josephson energy, both associated to a single JJ belonging to the superconducting loop, while $\hbar$ is the reduced Planck's constant. Beyond this frequency, the internal degrees of freedom of the device are activated and a more complex behavior appears. To overcome this problem, the external flux injected into the device will be composed of the sum of a signal oscillating at the driving frequency and a constant offset $\phi_{\rm ext} = \phi_0 + \Delta\phi\cos(\omega_d t)$. We will consider nondegenerate cavities in equation (1) to avoid uncorrelated photon generation at cavity resonance frequencies, an assumption that has been confirmed by a detailed quantum mechanical analysis of the effective lumped circuit element in Fig. 1c (see Supplementary Information). In addition, physical parameters such as capacitances, inductances, and Josephson energies should satisfy the rotating-wave approximation (RWA) applied to single and two-mode squeezing terms (see Methods).

Our protocol for generating entanglement requires neither direct[24] nor single cavity-bus mediated[25] qubit-qubit interaction. Instead, it consists in cooling down the system to its ground state, turning on the external driving flux $\phi_{\rm ext}$ and switching it off at time t_{SO}, when the maximal qubit entanglement is reached. The *concurrence* $\mathcal{C}$ is an entanglement measure for arbitrary two-qubit states, ranging from 0 for separable states to 1 for maximally entangled states[26]. Figure 2a shows that an almost maximally entangled state ($\mathcal{C}=0.97$) can be reached within $t_{SO}\approx 10-500$ ns, that is, for a wide range of realistic system parameters (see Supplementary Information). The density matrix of the produced Bell state is shown in Fig. 2b. We have also proven that entanglement generation is robust against small imperfections due to limited fabrication precision and imperfect ground state preparation.

In the framework of superconducting circuits, we can envision more complex configurations which generalize the concept of dynamical Casimir effect to the multipartite case. For instance, we consider three resonators connected to the ground via a SQUID, as shown in Fig. 3a. Injecting a fast-oscillating magnetic flux through the SQUID results in varying boundary conditions, which generate correlated photons

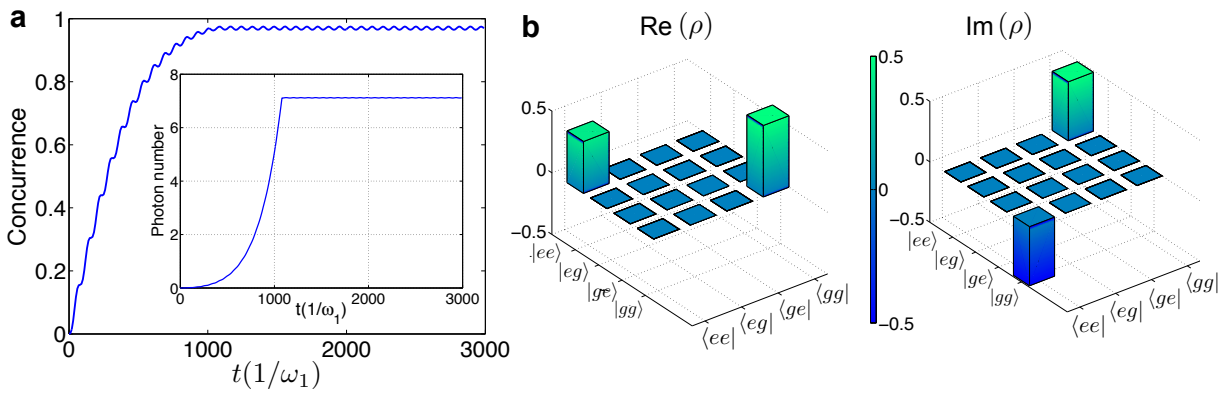

FIG. 2. **Two-qubit entanglement generation. a**, Concurrence and mean photon number as a function of time in units of the cavity frequency ω_1. Here, the chosen parameters are: $\omega_1/2\pi = 4$ GHz, $\omega_2/2\pi = 5$ GHz, the impedance for both cavities is $Z_0 = 50\Omega$, and the critical current of the SQUID junctions is $I_C = 1.1$ μA. Such parameters result in a squeezing parameter $\alpha_0 = \omega_1 \times 10^{-3}$. Each qubit is resonant with its corresponding cavity and they are coupled with the same interaction strength $g = 0.04\,\omega_2$. **b**, Real and imaginary part of the density matrix, ρ, associated to the two-qubit system. In this case, the system configuration allows us the generation of the Bell state $|\psi\rangle = (|ee\rangle + i|gg\rangle)/\sqrt{2}$ with fidelity $\mathcal{F} = |\langle\psi|\rho|\psi\rangle| = 0.99$.

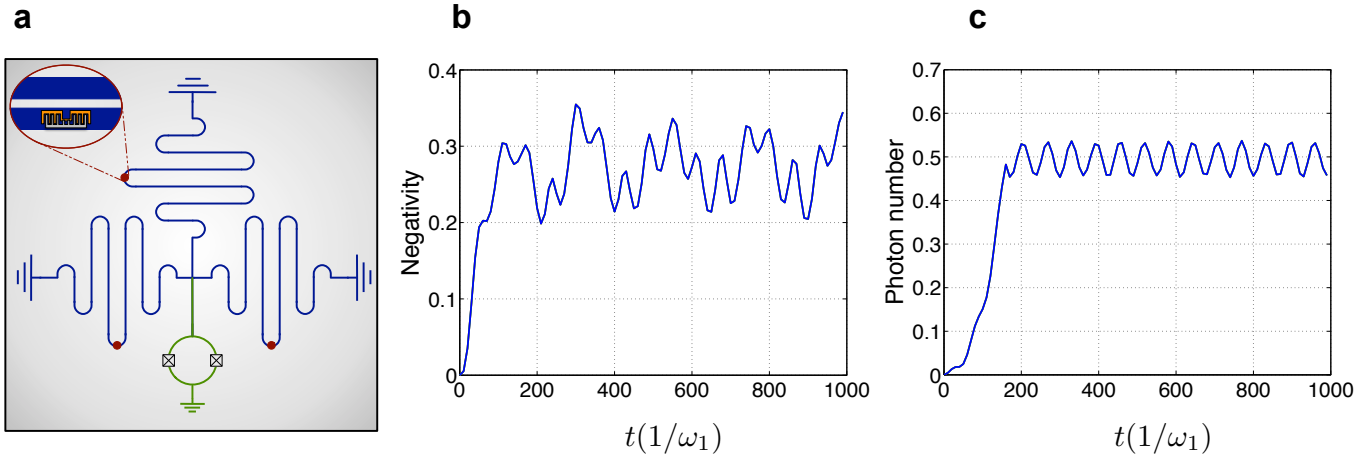

FIG. 3. **Three-qubit entanglement generation. a**, Three coplanar waveguide resonators are connected to the ground through a SQUID. Each resonator is coupled with a resonant transmon qubit. This scheme allows generation of GHZ-like entangled states, through a first-order process. Using this circuit design as a building-block, it is possible to explore more complex configurations and to build scalable cavity networks (see Supplementary Information). **b,** Negativity of the bipartite system obtained isolating one qubit from the set of the other two, as a function of time. Such figure of merit ranges from zero for separable to 0.5 for maximally entangled states. Here, we considered resonator frequencies of $\omega_1/2\pi = 3.8$ GHz, $\omega_2/2\pi = 5.1$ GHz and $\omega_3/2\pi = 7.5$ GHz. The SQUID is identical to the bipartite case and we use resonant qubits. The coupling parameters are homogeneous and their bare value is given by $\alpha_0 = 5\,\omega_1 \times 10^{-3}$. **c,** Average photon number in each cavity as a function of time. Due to the symmetric configuration the photon distribution is the same for the three cavities.

pairs distributed in the three cavity modes. Such a configuration has no direct analogy with optical cavities, as opposed to the bipartite case. The Hamiltonian describing the circuit of figure 3a is composed of the sum of three JC interactions and three time-dependent direct couplings between the field quadratures of each resonator pair

$$\mathcal{H} = \sum_{\ell=1}^{3}\left[\omega_\ell a_\ell^\dagger a_\ell + \frac{\omega_\ell^q}{2}\sigma_\ell^z + g_\ell\left(\sigma_\ell^+ a_\ell + \sigma_\ell^- a_\ell^\dagger\right)\right] \quad (3)$$
$$+ \sum_{\langle\ell,m\rangle}\alpha_{\ell m}(t)\left(a_\ell^\dagger + a_\ell\right)\left(a_m^\dagger + a_m\right).$$

When the external flux threading the SQUID is composed of the sum of three signals oscillating at the frequencies $\omega_{\ell m}^d = \omega_\ell + \omega_m$, we can isolate the two-mode squeezing terms as in equation (2).

Generating multipartite entanglement is a challenging task, since it requires multiqubit gates, whose operation fidelity is considerably lower than the single- or two-qubit gates. Numerical results on the negativity[27], shown in Fig. 3b, indicate that our circuit design can generate three-qubit entangled states. To prove that such state is not biseparable, we evaluate an entanglement monotone that detects only multipartite quantum correlations[28], called genuine multipartite en-

tanglement (GME) concurrence. Our results, $\max(\mathcal{C}_{\rm GME}) \approx 0.3$, confirm the existence of genuine multipartite entanglement. Furthermore, negative values of a Greenberger-Horne-Zeilinger (GHZ) witness[29] $\mathcal{W}_{\rm GHZ} = -0.06$ proves generation of (mixed) GHZ-like states, which belong to the most general entanglement class[13] (see Methods). Beyond the proposed model, our results show that superconducting circuits allow us to exploit the DCE physics as a useful resource for scalable quantum information protocols, generation of multipartite entanglement in artificial atoms, and as a building block for microwave quantum networks.

Methods

Single mode approximation. If the instantaneous resonant frequency of a given resonator follows the time-dependence $\omega(t) = \omega_0 + \delta\omega\cos(\omega_d t)$, cavity modes are well defined only under the condition $\delta\omega \ll \omega_0$. In our proposal, the frequencies of the cavity modes are obtained by solving the transcendental equation $kd\tan(kd) = L/L_s - C_s/C(kd)^2$ for the wave number k, where d is the length of the resonator. We called C_s, L_s and C, L the capacitance and inductance of the SQUID and of the resonator, respectively. Parameters used in our simulations assure that $\delta\omega/\omega_0 < 10^{-3}$, while interactions among different cavity modes, called mode mixing, are activated under the frequency-matching condition $\omega_d = \omega_a - \omega_b$. Cavity and driving frequencies can be chosen in order to make the relevant mode interact only with off-resonance overdamped modes. Circuit design allows each qubit to be resonantly coupled with a single cavity mode, where activation of higher modes due to the DCE mechanism can be neglected.

Driving Hamiltonian. In the interaction picture, the parametric processes induced by the SQUID lead to the Hamiltonian

$$\mathcal{H}_{\rm d}^I(t) = \hbar\cos(\phi_{\rm ext}/\varphi_0)\Big[\sum_{\ell=1}^{2}\alpha_\ell(a_\ell e^{-i\omega_\ell t} + a_\ell^\dagger e^{i\omega_\ell t})^2 - \tilde{\alpha}(a_1 e^{-i\omega_1 t} + a_1^\dagger e^{i\omega_1 t})(a_2 e^{-i\omega_2 t} + a_2^\dagger e^{i\omega_2 t})\Big], \quad (4)$$

where $\varphi_0 = \hbar/2e$ is the reduced flux quantum, and the coefficients α_ℓ and $\tilde{\alpha}$ are functions of the Josephson energy (E_J), the junction capacitance (C_J), the cavity parameters such as capacitance (C_ℓ) and inductance (L_ℓ). In order to apply the RWA to equation (4), the parameters α_ℓ and $\tilde{\alpha}$ must be much smaller than cavity frequencies ω_ℓ. In this case, if we consider $\phi_{\rm ext} = \phi_0 + \Delta\phi\cos(\omega_d t)$ with $\Delta\phi$ a small flux amplitude and $\omega_d = \omega_1 + \omega_2$, one can neglect off-resonance processes, leading to equation (2).

Entanglement measures. The concurrence $\mathcal{C}$ is an entanglement monotone of a given bipartite mixed state ρ, namely, the minimum average entanglement of an ensemble of pure states that represents ρ. For an arbitrary two-qubit state the concurrence reads

$$\mathcal{C}(\rho) = \max\{0, \lambda_1 - \lambda_2 - \lambda_3 - \lambda_4\}, \quad (5)$$

where λ_i are the eigenvalues, in decreasing order, of the Hermitian matrix $R = \sqrt{\sqrt{\rho}\tilde{\rho}\sqrt{\rho}}$, where $\tilde{\rho} = \sigma_y \otimes \sigma_y \rho^* \sigma_y \otimes \sigma_y$. For the three-partite case we use the negativity defined as

$$\mathcal{N}(\rho) = \frac{||\rho^{T_A}||_1 - 1}{2} \quad (6)$$

where $||\rho^{T_A}||_1$ is the trace-norm of the partial transpose of the bipartite mixed state ρ. The negativity is an entanglement monotone that estimates the bipartite entanglement shared between the two subsystems of any possible bipartition, it ranges from zero for separable to $1/2$ for maximally entangled states. In addition, the detection of genuine multipartite entanglement is carried out by $\mathcal{C}_{\rm GME}$, a figure of merit that is the result of an optimization process over all decomposable witnesses $W = P + Q^{T_A}$, where P and Q are positive semidefinite[28]. This entanglement monotone detects only genuine multipartite entanglement, being zero for separable and biseparable states. In order to identify the entanglement class of three-qubit states, we considered the following entanglement witness: $\mathcal{W}_{\rm GHZ} = 3/4\,\mathbb{I} - P_{\rm GHZ}$, where $P_{\rm GHZ}$ is the projector onto $|{\rm GHZ}\rangle$. Negative values for ${\rm Tr}[\rho\mathcal{W}_{\rm GHZ}]$ imply that for any decomposition $\rho = \sum_j p_j\rho_j$, at least one ρ_j is a GHZ state and, hence, ρ belongs to the GHZ entanglement class. Given that local operations do not change the entanglement class, the witness can be optimized by minimizing the quantity ${\rm Tr}\left[F\rho F^\dagger\mathcal{W}_{\rm GHZ}\right]$, where $F = F_1 \otimes F_2 \otimes F_3$ and F_i are arbitrary single-qubit SLOCC operations.

[1] Lamb, W. E. & Retherford, R. C. Fine structure of the Hydrogen Atom by a Microwave Method. *Phys. Rev.* **72,** 241 (1947).

[2] Peskin, M. E. & Schroeder, D. V. *An Introduction to Quantum Field Theory* (Westview Press, 1995).

[3] Moore, G. T. Quantum theory of the electromagnetic field in a variable-length one-dimensional cavity. *J. Math. Phys.***11,** 2679 (1970).

[4] Wilson, C. M., Johansson, G., Pourkabirian, A., Simoen, M., Johansson, J. R., Duty, T., Nori, F. & Delsing, P. Observation of the dynamical Casimir effect in a superconducting circuit. *Nature* **479,** 376-379 (2011).

[5] Lähteenmäki, P., Paraoanu, G. S., Hassel, J. & Hakonen, P. J. Dynamical Casimir effect in a Josephson metamaterial. *Proc. Natl. Acad. Sci. U.S.A.* **110**, 4234 (2013).

[6] Casimir, H. B. G. On the attraction between two perfectly conducting plates. *Proc. K. Ned. Akad. Wet. B* **51,** 793 (1948).

[7] Lamoreaux, S. K. Demonstration of the Casimir Force in the 0.6 to 6μm Range. *Phys. Rev. Lett.* **78,** 5 (1997).

[8] Mohideen, U. & Roy, A. Precision Measurement of the Casimir Force from 0.1 to 0.9μm. *Phys. Rev. Lett.* **81,** 4549 (1998).

[9] Einstein, A., Podolsky, B., & Rosen, N. Can Quantum-Mechanical Description of Physical Reality Be considered Complete? Phys. Rev. **47**, 777 (1935).

[10] Blais, A., Huang, R. S., Wallraff, A., Girvin, S. M. & Schoelkopf, R. J. Cavity quantum electrodynamics for superconducting electrical circuits: An architecture for quantum computation. *Phys. Rev. A* **69**, 062320 (2004).

[11] Chiorescu, I., Bertet, P., Semba, K., Nakamura, Y., Harmans, C. J. P. M. & Mooij, J. E. Coherent dynamics of a flux qubit coupled to a harmonic oscillator. *Nature (London)* **431**, 159 (2004).

[12] Wallraff, A., Schuster, D. I., Blais, A., Frunzio, L., Huang, R. S., Majer, J., Kumar, S., Girvin, S. M & Schoelkopf, R. J. Circuit Quantum Electrodynamics: Coherent Coupling of a Single Photon to a Cooper Pair Box. *Nature (London)* **431**, 162 (2004).
[13] Acín, A., Bruß, D., Lewenstein, M. & Sanpera, A. Classification of Mixed Three-Qubit States. *Phys. Rev. Lett.* **87**, 040401 (2001).
[14] Ladd, T. D., Jelezko, F., Laflamme, R., Nakamura, Y., Monroe, C. & OBrien, J. L. Quantum Computers. *Nature (London)* **464**, 45 (2010).
[15] Wilhelm, F. K. & Clarke, J. Superconducting quantum bits. *Nature* **453**, 1031 (2008).
[16] Devoret, M. & Schoelkopf, R. J. Superconducting Circuits for Quantum Information: An Outlook. *Science* **339**, 1169 (2013).
[17] Bruschi, D. E. *et al.* Towards universal quantum computation through relativistic motion. Preprint at *http://arxiv.org/abs/1311.5619* , (2013).
[18] Wallquist, M., Shumeiko, V. S. & Wendin, G. Selective coupling of superconducting charge qubits mediated by a tunable stripline cavity, *Phys.Rev. B* **76,** 224506 (2006).
[19] Bouchiat, V., Vion, D., Joyez, P., Esteve, D. & Devoret, M. H. Quantum coherence with a single Cooper pair. *Phys. Scr.* **T76**, 165 (1998).
[20] Mooij, J. E., Orlando, T. P., Levitov, L., Tian, L., van der Wal, C. H., & Lloyd, S. Josephson Persistent-Current Qubit. *Science* **285**, 1036 (1999).
[21] Martinis, J. M., Devoret, M. H. & Clarke, J. Energy-Level Quantization in the Zero-Voltage State of a Current-Biased Josephson Junction. *Phys. Rev. Lett.* **55**, 1543 (1985).
[22] Koch, J., Yu, T. M., Gambetta, J., Houck, A. A., Schuster, D. I., Majer, J., Blais, A., Devoret, M. H., Girvin, S. M. & Schoelkopf, R. J. Charge-insensitive qubit design derived from the Cooper pair box. *Phys. Rev. A* **76**, 042319 (2007).
[23] Orlando, T. P. & Delin, K. A. *Foundations of applied superconductivity* (Addison-Wesley, 1991).
[24] Steffen, M. *et al*. Measurement of the entanglement of two superconducting qubits via state tomography. *Science* **313**, 1423 (2006).
[25] DiCarlo, L. *et al*. Demonstration of Two-Qubit Algorithms with a Superconducting Quantum Processor. *Nature* **460**, 240 (2009).
[26] Wootters, W. K. Entanglement of Formation of an Arbitrary State of Two Qubits. *Phys. Rev. Lett.* **80**, 2245 (1998).
[27] Vidal, G. & Werner, R. F. Computable measure of entanglement. *Phys.Rev. A* **65,** 032314 (2002).
[28] Jungnitsch , B., Moroder, T. & Gühne, O. Taming Multiparticle Entanglement. *Phys. Rev. Lett.* **106**, 190502 (2011).
[29] Kiesel, N., Schmid, C., Tóth, G., Solano, E. & Weinfurter, H. Experimental Observation of Four-Photon Entangled Dicke State with High Fidelity. *Phys. Rev. Lett.* **98**, 063604 (2007).
[30] Paik, H. *et al.* Observation of High Coherence in Josephson Junction Qubits Measured in a Three-Dimensional Circuit QED Architecture *Phys. Rev. Lett.* **107**, 240501 (2011).
[31] Chang, J. B. *et al.* Improved superconducting qubit coherence using titanium nitride *Appl. Phys. Lett.* **103**, 012602 (2013).

Acknowledgments We thank Géza Tóth and Jens Siewert for useful discussions. The authors acknowledge support from Spanish MINECO FIS2012-36673-C03-02; Ramón y Cajal Grant RYC-2012-11391; UPV/EHU UFI 11/55; Basque Government IT472-10; CCQED, PROMISCE, SCALEQIT EU projects; and the Swedish Research Council.

SUPPLEMENTARY INFORMATION

In this supplementary material, we detail the derivation of the quantum model of the circuit design showed in Fig. 1b of the main text, and we briefly discuss possible future development of our work. In section I, we derive the full quantum Hamiltonian that describes the bipartite configuration. In section II, we show how to extend the model to the multipartite case, and how our proposal can be used as a building block to implement highly correlated cavity networks for quantum information and quantum simulation.

I. QUANTUM MODEL

In this section, we derive the quantum model of the circuit design proposed in Fig. 1b of the main text. We restrict to consider the bare resonators, an effective interaction with resonant qubits can be added at the end of the derivation. Let us consider a circuit composed of two transmission line resonators (TLS), connected to the ground through the same superconducting quantum interference device (SQUID), as shown in figure 4. A SQUID is a superconducting loop interrupted by two Josephson junctions (JJ). Here we take the two JJs that constitute the SQUID to be identical: under this assumption, the SQUID effectively behaves as a single JJ[1], namely, as a non-linear tunable inductance shunted by a small capacitance. We also assume that the JJs are such that their Josephson energy is much bigger than their charge energy $E_J \gg E_C$. In order to write the system classical Lagrangian, we will use a discrete description of the TLSs: each resonator will be represented by an infinite series of LC oscillators of

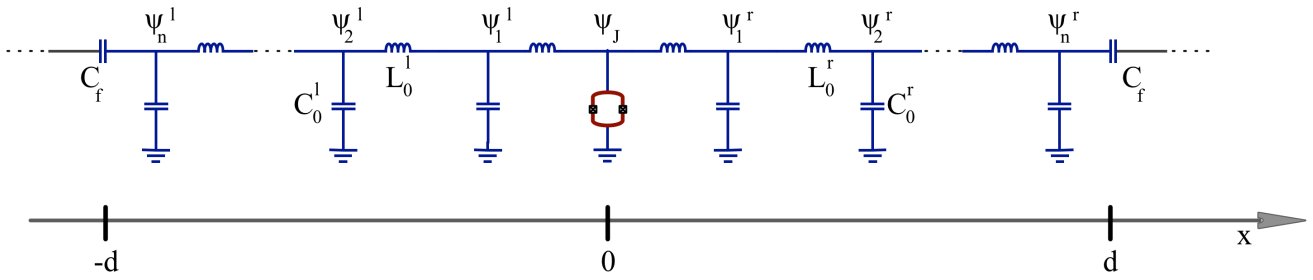

FIG. 4. **Sketch of the system.** Two transmission line resonators are connected to the same edge of a grounded SQUID. The SQUID low impedance imposes a voltage node at $x = 0$. Each resonator is coupled with an external line (not considered here) needed for reading the cavity.

infinitesimal length Δx. The system Lagrangian can be then written as

$$\mathcal{L} = \frac{1}{2}\sum_i \left\{ \Delta x C_0^l \left(\dot{\psi}_i^l\right)^2 + \frac{1}{\Delta x L_0^l}\left(\psi_{i+1}^l - \psi_i^l\right)^2 \right\} \tag{7}$$

$$+ \frac{1}{2}\sum_i \left\{ \Delta x C_0^r \left(\dot{\psi}_i^r\right)^2 + \frac{1}{\Delta x L_0^r}\left(\psi_{i+1}^r - \psi_i^r\right)^2 \right\} \tag{8}$$

$$+ \frac{1}{2} C_J \left(\dot{\psi}_J\right)^2 - \frac{E_J\left(\phi_{\text{ext}}\right)}{2\varphi_0^2}\psi_J^2. \tag{9}$$

We defined the magnetic flux $\psi_i^{l/r}$ in the i-th inductor of the left/right resonator as the time integral of the instantaneous voltage v_i across the element: $\psi_i^{l/r}(t) = \int_0^t v_i(\tau)d\tau$. The capacitance and inductance per unit of length are denoted by $C_0^{l/r}$ and $L_0^{l/r}$, respectively. Variables and constants with the subscript J refer to the SQUID; notice that C_J and L_J represent the total capacitance and inductance of the SQUID, which will be described by means of a lumped-element model also in the continuum limit ($\Delta x \to 0$). We defined the reduced magnetic flux as $\varphi_0 = \phi_0/2\pi$, where ϕ_0 is the magnetic flux quantum. The inductance of the SQUID depends on the external flux ϕ_{ext} threading the device: $L_J = \frac{\varphi_0^2}{E_J(\phi_{\text{ext}})}$, where $E_J(\phi_{\text{ext}}) = 2E_J\left|\cos\left(\frac{\phi_{\text{ext}}}{2\varphi_0}\right)\right|$. The Josephson energy E_J and the critical current I_c are directly related $E_J = I_c\varphi_0$.

A. Spatial modes

In the bulk of each resonator the equation of motion is given by (for the sake of simplicity we omit the superscript *l*/*r*)

$$C_0\ddot{\psi}_i(t) = \frac{1}{\Delta x}\left\{\frac{\psi_{i+1}(t) - \psi_i(t)}{\Delta x L_0} - \frac{\psi_i(t) - \psi_{i-1}(t)}{\Delta x L_0}\right\} \tag{10}$$

which, in the continuum limit $\Delta x \to 0$, reduces to

$$\ddot{\psi}(x,t) = v\,\frac{\partial^2}{\partial x^2}\psi(x,t)\Big|_{x=0} \qquad \text{where} \qquad v = \frac{1}{\sqrt{C_0 L_0}}. \tag{11}$$

The differential equation (11) can be solved using the usual variable separation ansatz $\psi(x,t) = f(x)\phi(t)$, with $f(x) = \alpha\cos(kx) + \beta\sin(kx)$, $\phi(t) = ae^{-i\omega t} + be^{i\omega t}$, and $\omega = k/\sqrt{L_0 C_0}$. The electrical boundary conditions at the far left and far right extremities are established by the capacitances C_f, which mediate the coupling with external transmission lines. This capacitive coupling can be made very small and its contribution to the resonator modes is negligible. Following a standard procedure, we will use open boundary conditions in order to evaluate the resonator modes, the interaction with the environment can be then described by means of a small effective coupling.

$$\frac{\partial\psi^l(x)}{\partial x}\Big|_{x=-d} = 0 \qquad \text{and} \qquad \frac{\partial\psi^r(x)}{\partial x}\Big|_{x=d} = 0. \tag{12}$$

The equation of motion for the dynamical variable ψ_J corresponds to the Kirchhoff law of current conservation at the central node ($x = 0$)

$$C_J \ddot{\psi}^2(0,t) + \frac{E_J\left(\phi_{\text{ext}}\right)}{\varphi_0^2}\psi(0,t) = \frac{1}{L_0^l}\left.\frac{\partial \psi^l(x)}{\partial x}\right|_{x=o} + \frac{1}{L_0^r}\left.\frac{\partial \psi^r(x)}{\partial x}\right|_{x=0}. \tag{13}$$

Now, given that the resonator inductances are much bigger than the SQUID inductance $L_J = \varphi_0^2/E_J\left(\phi_{\text{ext}}\right)$, the terms on the right side of equation (13) are very small compared to the inductive contribution of the SQUID. This mathematical statement has the following physical interpretation: the SQUID is a low-impedance element, therefore most of the current coming either from the left or from the right will flow through the SQUID directly to the ground, without crossing the other resonator. In other words, the presence of one resonator does not perceptibly modify the mode structure of the other one, although a small inductive coupling between them can be introduced from equation (13). This allows us to define separated modes for the two resonators, which are constrained to satisfy the boundary condition

$$(k\,d)\tan\left(k\,d\right) = \frac{C_J}{C}\left(k\,d\right)^2 - \frac{L}{L_J}. \tag{14}$$

This equation holds for both resonators, we omitted the superscripts l/r and we defined the total capacitance $C = C_0\,d$ and total inductance $L = L_0\,d$. Notice that modifying the external flux ϕ_{ext} results in a variation of the SQUID effective inductance L_J, and so in a modification of the boundary condition (14). Finally, the resonator frequencies can be found solving the differential equations (11), being the boundary conditions given by (12) and by the solution of the transcendental equation[2] (14).
For didactical purpose, we observe that a good approximation to the resonator modes can be found assuming that at $x = 0$ there is a voltage node, namely $\psi(0,t) = 0$. Under this assumption, the system is composed of two independent $\lambda/4$ resonators

$$f(x) = \sqrt{2}\sum_n \sin\left(k_n\,x\right) \qquad \text{where} \quad k_n = \frac{\pi}{d}\left(\frac{1}{2} + n\right). \tag{15}$$

B. Hamiltonian

Now, we write the system Lagrangian exploiting the stationary spatial solutions found in section I A. Integrating equations (7) and (8) over the spatial degree of freedom, in the continuum limit, we obtain the Lagrangian of the free resonators

$$\mathcal{L}_0 = \sum_{\nu=l,r}\sum_n \left\{\frac{C^\nu}{2}\left[\dot{\phi}_n^\nu(t)\right]^2 - \frac{1}{L^\nu}\left[\phi_n^\nu(t)\right]^2\right\}, \tag{16}$$

where the index ν identifies resonator, while n runs over the spatial eigenmodes (and so, over the frequencies). We are interested in the dynamics of two level quantum systems that are embedded in the resonators. These qubits effectively interact only with one mode of each cavity, hence, hereafter we will restrict to consider one mode per resonator. This treatment is valid under the condition that the oscillation of the boundary conditions do not make resonant interaction terms between the relevant mode and the other ones.
The effective interaction between the modes ϕ^l and ϕ^r can be found isolating the variable $\phi(0,t)$ in equation (13) and replacing it in the SQUID contribution to the system Lagrangian (equation (9))

$$\mathcal{L}_{int} = -\frac{\varphi_0^2}{E_J\left(\phi_{\text{ext}}\right)}\left\{\frac{1}{L_0^l}k^l\phi^l(t) + \frac{1}{L_0^r}k^r\phi^r(t)\right\}^2. \tag{17}$$

Now we assume that the prefactor of the previous equation is oscillating with a frequency such that only the cross-interaction term will be relevant in the Hamiltonian dynamics. This regime is accessible when the resonators are off resonance and the difference between their frequencies is much bigger than the coupling strength. We will show that the considered regime of parameters allows such approximation. Defining the conjugate momentum $q^{l/r} = \partial\mathcal{L}_{tot}/\partial\dot{\phi}^{l/r}$, we find the system Hamiltonian

$$\mathcal{H} = \sum_{\nu=l,r}\left\{\frac{1}{2C_\nu}q_\nu^2(t) + \frac{\omega_\nu^2 C_\nu}{2}\phi_\nu^2(t)\right\} - \frac{2\varphi_0^2}{E_J\left(\phi_{\text{ext}}\right)}\frac{\omega_l\omega_r}{Z_l Z_r}\phi_l\phi_r, \tag{18}$$

where we defined the impedance as $Z_\nu = \sqrt{L_\nu/C_\nu}$. Now, we perform the usual quantization process and define ladder operators

$$[\phi_\nu, q_\nu] = i\hbar \qquad , \qquad \phi_\nu = \sqrt{\frac{\hbar}{2\omega_\nu C_\nu}}\left(a_\nu^\dagger + a_\nu\right) \qquad , \qquad q_\nu = i\sqrt{\frac{\hbar C_\nu\omega_\nu}{2}}\left(a_\nu^\dagger - a_\nu\right). \tag{19}$$

Finally, we can write the system quantum Hamiltonian as

$$\mathcal{H}/\hbar = \omega_l a_l^\dagger a_l + \omega_r a_r^\dagger a_r - \frac{\varphi_0^2}{E_J\left(\phi_{\text{ext}}\right)}\sqrt{\frac{\omega_l\omega_r}{C_l C_r}}\frac{1}{Z_l Z_r}\left(a_l^\dagger + a_l\right)\left(a_r^\dagger + a_r\right). \tag{20}$$

C. Two-mode squeezing

Observe that, as stated in the main text, when the driving frequency is comparable to the SQUID plasma frequency, the device can not be considered as a passive element and a more complex behaviour emerges. The SQUID plasma frequency is defined as $\omega_p = \sqrt{1/C_J L_J}$, so ω_p becomes smaller as the external flux get closer to $\phi_{\text{ext}}/2\varphi_0 = \pi/2$. To overcome this problem, we consider an external flux which is oscillating with small variation Δ around a fixed offset $\bar{\phi}$. In this way, with the physical parameters we considered, the SQUID plasma frequency is much bigger than ω_d for every value of $\phi_{\text{ext}}(t)$ during the time evolution. Such condition allows us to expand the coupling parameter in the interaction term of equation (20)

$$\frac{\phi_{\text{ext}}}{2\varphi_0} = \bar{\phi} + \Delta\cos\left(\omega_d t\right) \qquad \Longrightarrow \qquad \frac{1}{E_J\left(\phi_{\text{ext}}\right)} \approx \frac{1}{\cos\bar{\phi}} + \frac{\sin\bar{\phi}}{\cos^2\bar{\phi}}\,\Delta\,\cos\left(\omega_d t\right). \tag{21}$$

Hence, the interaction term of the system Hamiltonian can be written, in the Schrödinger picture, as the sum of a constant and a time-dependent term

$$\mathcal{H}/\hbar = \omega_l a_l^\dagger a_l + \omega_r a_r^\dagger a_r + \eta\left(a_l^\dagger + a_l\right)\left(a_r^\dagger + a_r\right) + \alpha_0\left(e^{i\omega_d t} + e^{-i\omega_d t}\right)\left(a_l^\dagger + a_l\right)\left(a_r^\dagger + a_r\right), \tag{22}$$

with

$$\eta = \frac{\varphi_0^2}{2E_J\cos\bar{\phi}}\sqrt{\frac{\omega_l\omega_r}{C_l C_r}}\frac{1}{Z_l Z_r} \qquad \text{and} \qquad \alpha_0 = \frac{\varphi_0^2}{4E_J}\frac{\sin\bar{\phi}}{\cos^2\bar{\phi}}\sqrt{\frac{\omega_l\omega_r}{C_l C_r}}\frac{1}{Z_l Z_r}\Delta. \tag{23}$$

When the detuning between the resonators is large compared to the coupling parameters $\eta, \alpha_0 \ll |\omega_l - \omega_r|$, we can perform the rotating wave approximation and neglect all terms that are fast-oscillating in the interaction picture. If we choose the external driving to match the sum of the resonators frequencies $\omega_d = \omega_l + \omega_r$, the interaction Hamiltonian will reduce to a two-mode squeezing term

$$\mathcal{H}/\hbar = \omega_l a_l^\dagger a_l + \omega_r a_r^\dagger a_r + \alpha_0\left(e^{-i\omega_d t}a_l^\dagger a_r^\dagger + e^{i\omega_d t}a_l a_r\right). \tag{24}$$

II. MULTIPARTITE CASE

Consider a circuit scheme such that n resonators are connected to the ground through the same SQUID, as shown in figure 6a for $n = 4$. Equation (11) still holds in the bulk of each resonator, and the boundary conditions (12) are still valid. On the other hand, the Kirchhoff's law of current conservation (13) must be extended to include the contribution of every branch of the circuit

$$C_J\ddot{\psi}^2(0,t) + \frac{E_J\left(\phi_{\text{ext}}\right)}{\varphi_0^2}\psi(0,t) = \sum_\nu \frac{1}{L_0^\nu}\left.\frac{\partial\psi^\nu(x)}{\partial x}\right|_{x=o}. \tag{25}$$

As far as the resonator inductances are much larger than the SQUID inductance, we can still treat the system as composed of independent resonators, interacting through a small current-current coupling. In this case, resonator spatial eigenmodes can be found following the same procedure we used in the bipartite case. Neglecting a small capacitive contribution, the term in the Lagrangian which describes the current-current coupling can be written as

$$\mathcal{L}_{int} = -\frac{\varphi_0^2}{E_J\left(\phi_{\text{ext}}\right)}\left\{\sum_\nu \frac{1}{L_0^\nu}k^\nu\phi^l(t)\right\}^2. \tag{26}$$

In a quantum description of such system, these interactions result in single-mode drivings and two-mode interactions between the field quadratures

$$\mathcal{H}_I = \sum_\nu \alpha_\nu(t)\left(a_\nu^\dagger + a_\nu\right)^2 + \sum_{\nu,\mu}\beta_{\nu\mu}(t)\left(a_\nu^\dagger + a_\nu\right)\left(a_\mu^\dagger + a_\mu\right), \tag{27}$$

where the parameters $\alpha_\nu(t)$ and $\beta_{\nu\mu}(t)$ depend on the external flux $\phi_{\rm ext}(t)$ threading the SQUID, and they are all small compared to the resonator characteristic frequencies. The time-dependence of $\phi_{\rm ext}(t)$ establishes which terms of equation (27) will have a non-negligible contribution to the system dynamics. When the external flux is given by the sum of signals oscillating at different frequencies, with small variations Δ_i, around a constant off-set $\bar{\phi}$

$$\frac{\phi_{\rm ext}}{2\varphi_0} = \bar{\phi} + \Delta_1 \cos\left(\omega_{d1} t\right) + \Delta_2 \cos\left(\omega_{d2} t\right) + \ldots, \tag{28}$$

with $\Delta_i \ll \bar{\phi}$, we can generalize the method used in equation (28)

$$\frac{1}{E_J\left(\phi_{\rm ext}\right)} \approx \frac{1}{\cos\bar{\phi}} + \frac{\sin\bar{\phi}}{\cos^2\bar{\phi}}\,\Delta_1\,\cos\left(\omega_{d1} t\right) + \frac{\sin\bar{\phi}}{\cos^2\bar{\phi}}\,\Delta_2\,\cos\left(\omega_{d2} t\right) + \ldots \tag{29}$$

Hence, controlling the external flux allows to turn on and off single- and two-mode squeezing terms, as well as linear couplings between the resonators.

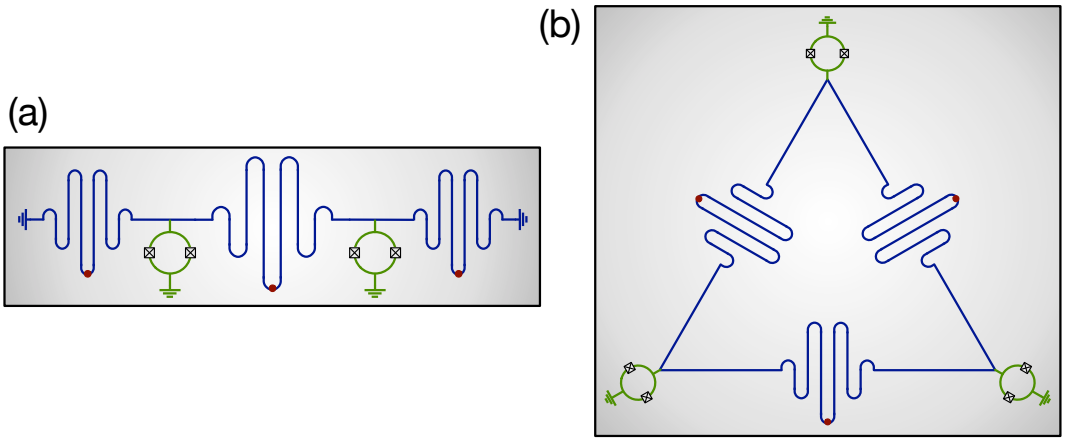

FIG. 5. **Tripartite setups. (a)** Linear array of three resonators with near-neighbour couplings. **(b)** Three SQUIDs in a triangular configuration. In this case, it is possible to control individually every current-current interaction in real time.

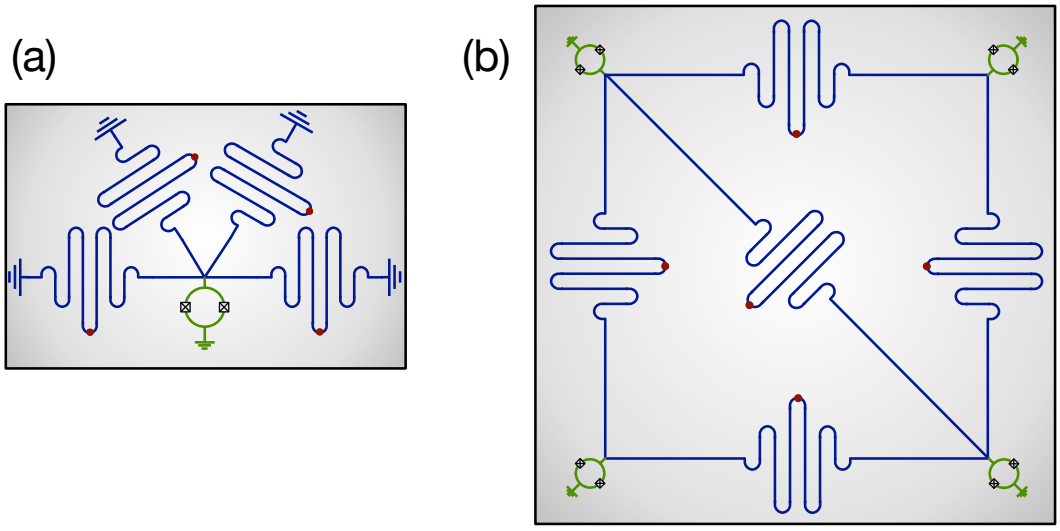

FIG. 6. **Multipartite case.** Complex cavity configurations which deploy the dynamical Casimir physics in order to implement highly-correlated quantum networks.

A. Outlook

Our theoretical analysis shows that fast-oscillating boundary conditions can generate a maximum entangled state of two qubits, in a non trivial way. This result demonstrates that the dynamical Casimir effect (DCE) represents a valuable, so far overlooked resource for quantum information science. The implementation of quantum resonators ruled by fast-oscillating boundary conditions in superconducting circuits discloses the possibility of generalizing the dynamical Casimir physics to multipartite systems. Accordingly, we have theoretically proven that the DCE allows generation of three-qubit entangled states belonging to the GHZ class, i.e., to the most general class of genuine multipartite entanglement in the three-partite case.

Our proposal can be used as a building block to realize more complex circuit configurations, which exploit the dynamical Casimir physics in order to generate and distribute quantum correlations. Figure 5 shows two possible configurations of three-cavity setups: a linear array, box (a), and a triangular configuration, box (b). In the multipartite configuration presented in the main text (figure 3a), two-body interactions links resonators pairwise, while the schemes of figure 5 lead to first-neighbour couplings.The linear array is interesting since it can be easily scaled to higher number of resonators. The triangular configuration allows real-time control of the inhomogeneities in the couplings, due to the presence of three SQUIDs. Notice that, in the case in which both ends of a resonator are connected to a SQUID, the configuration of the spatial modes is such that there are voltage nodes at both extremities. Figure 6a shows a direct generalization of the three-partite scheme studied in the main paper, in which four cavities are involved. Such configuration is the most natural candidate to generate symmetric genuine multipartite entangled states of more artificial atoms. Finally, in figure 6b it can be found an example of complex Casimir network, which shows the flexibility of the present proposal.

[1] Likharev, K. K. *Dynamics of Josephson Junctions and Circuits* (Gordon, Amsterdam, 1986).
[2] Wallquist, M., Shumeiko, V. S. & Wendin, G. Selective coupling of superconducting charge qubits mediated by a tunable stripline cavity, *Phys.Rev. B* **76,** 224506 (2006).